ARTICLES

Experimental study of the reaction $pp \rightarrow pp\pi^0$ in the energy range 600–900 MeV

V. P. Andreev, A. V. Kravtsov, M. M. Makarov, V. I. Medvedev, V. I. Poromov, V. V. Sarantsev, S. G. Sherman, G. L. Sokolov, and A. B. Sokornov
Petersburg Nuclear Physics Institute, Gatchina 188350, Russia
(Received 15 December 1993)

The detailed study of the reaction $pp \rightarrow pp\pi^0$ was carried out at seven energies of the incident proton in the region 600–900 MeV. Energy spectra, angular, and effective mass distributions were analyzed. The analysis was performed in the framework of the one-pion exchange model. Taking into account only the P_{33} wave in the pole diagrams allows one to obtain good agreement with experimental data on various differential distributions. At the same time the predictions for total cross sections are much lower than the experimental data.

PACS number(s): 13.75.Cs, 25.40.Ep

I. INTRODUCTION

The process of pion production is the main inelastic one in NN interactions at energies below 1 GeV. Despite the fact that a lot of experiments have been performed, many questions on this process are not yet answered. One of them is a question of the contribution of the isoscalar (I=0) channel to the inelastic neutron-proton collisions. Since the neutron-proton scattering amplitude contains both isoscalar and isovector (I=1) contributions, a detailed investigation of the neutral pion production in pp collisions, as a first step, might give the most accurate information on the isovector channel.

Various theoretical models, more or less successful, arose while the data on the pion production in NN collisions were accumulating. One of them was the semiphenomenological isobar model by Mandelstam [1] which assumed that the pion production is dominated by formation of the intermediate $N\Delta$ state following decay of the isobar to a nucleon and a pion. The theory supposed the energy independence of the amplitude and contradicted experimental data at energies higher than 700 MeV. An earlier peripheral or one-pion exchange (OPE) model [2] assumed the dominance of the one-pion exchange term in the inelastic amplitude. Pole diagram matrix elements were calculated using the uncertain before-hand form factor, the interference between diagrams being neglected. The form factor function was obtained then by fitting the experimental data, so actually this was a semiphenomenological model. Its predictions were in rather good agreement with rough measurements of the differential cross sections in the energy range 800–1300 MeV. It was one of the reasons why both theoretical and experimental investigations in this energy range were not very popular.

The situation changed drastically when structures were observed in the energy dependence of the difference of the proton-proton total cross sections in the pure spin states, $\Delta\sigma_L$ and $\Delta\sigma_T$ [3]. One of the intriguing possible explanations of these structures was a hypothesis of the dibaryon resonances. Intensive investigations in this field enriched considerably both the theory of the pion production and experimental data, though the status of these dibaryons is not clarified yet [4].

After the work in Refs. [5–7] it became evident that the modifications of the one-pion exchange model used there describe rather well (with an accuracy of 5–10%) the differential spectra of secondaries of the $pp \rightarrow pn\pi^+$ reaction which presented the most part of experimental information that time. The total cross sections were predicted to be a little lower than observed [6]. For other reactions,e.g., $pp \rightarrow pp\pi^0$, the discrepancies between the theory and experiment [8–12] were larger.

It should be noted that the experimental data on the $pp \rightarrow pp\pi^0$ reaction are much more scarce than those for $pp \rightarrow pn\pi^+$ channel. The only data on the spectra of secondaries in the energy range 700–1000 MeV are presented in Ref. [13], the statistics being rather poor. KEK data [11] contain information only on the total cross sections with an energy step of about 100 MeV, which makes it difficult to analyze correctly the energy behavior of the total cross sections in the region of the dibaryon resonances expected. For this reason, we consider it important to perform more accurate measurements of the cross sections with an energy step about 40–50 MeV and to compare carefully the differential distributions of secondaries in the $pp \rightarrow pp\pi^0$ reaction with the predictions of the modern OPE model. Such comparisons would allow one to see strong and weak sides of this simplest theoretical model, as well as to judge the necessity of some additional nonperipheral mechanisms of the pion production in NN collisions. Our results on the total cross sections of the reaction were published in [12]. Here we present the investigation of the differential spectra and their comparison with the advanced OPE model [7].

II. EXPERIMENT

The measurements were performed at the PNPI synchrocyclotron with help of the 35 cm hydrogen bubble

TABLE I. Numbers of events and cross section values of the $pp \to pp\pi^0$ reaction.

P (MeV/c)	1217	1279	1341	1389	1437	1485	1536
N_{events}	642	621	880	993	899	1000	1318
$\sigma_{pp\pi^0}$ (mb)	2.07±0.09	2.85±0.13	3.31±0.19	3.70±0.14	3.73±0.15	3.96±0.15	4.20±0.15
$\sigma_{\text{exp}}/\sigma_{\text{OPE}}$	2.55	2.21	1.82	1.67	1.46	1.39	1.35

chamber disposed in the 1.48 T magnetic field. The proton beam after the corresponding absorber was formed by three bending magnets and by eight quadrupole lenses. The value of the incident proton momentum was inspected independently by the kinematics of the elastic scattering events. The accuracy of the incident momentum value was ±2 MeV/c, the momentum spread being 4–5 % (FWHM). A total of 3×10^5 stereo frames were obtained at seven proton energies. The larger number of pictures taken at low energies was inversely proportional to the expected cross section value for the neutral pion production.

According to the kinematics of the pion production in NN collisions, laboratory angles of secondary protons are in the forward hemisphere, the maximum angle being not larger than 60° at our energies. For this reason we selected two-prong events with track angles in the plane of the film not larger than 60°.

Events so selected could belong not only to the neutral pion production, but also to the elastic pp scattering or to the π^+ production reaction. The events in the fiducial volume of the chamber were measured and geometrically reconstructed. The identification of the events was performed on the strength of the χ^2 criterion, the confidence level being equal to 1%. If the event had good χ^2 for the elastic version (4C fit) it was considered to be an elastic one. If both inelastic versions revealed good χ^2, we used a visual estimate of the ionization density to distinguish between the proton and pion.

Standard bubble chamber procedure was used to obtain absolute cross sections [12]. Absolute values were measured with an accuracy of 3–4 %, which is the most accurate measurement in the energy range in question. The cross sections obtained for the $pp \to pp\pi^0$ reaction are given in Table I together with the statistics at every proton momentum and the ratios of the experimental values to the OPE model predictions calculated here.

III. ONE-PION EXCHANGE MODEL

According to the OPE model [2], the main role in the reaction $NN \to NN\pi$ belongs to the pole diagrams (Fig. 1). The matrix element corresponding to any diagram can be presented as a product of three factors: the propagator, the amplitude of the πN scattering, and the πNN vertex function

$$M_i \sim \frac{1}{k_i^2 + \mu^2} \Im(z_i, y_i^2; k_i^2) G(k_i^2), \tag{1}$$

where z_i is the total energy of the πN system, y_i^2 is the square of the four-momentum transferred in the πN-scattering vertex, k_i^2 is the square of the four-momentum of the virtual pion, and μ^2 is the pion mass squared.

The form factor function of the πNN vertex taking into account the nonpole diagrams contribution was not determined in the frame of the OPE model. On the other side, for the form factor the following form was suggested:

$$G(k_i^2) = \alpha\mu^2/[k_i^2 + (\alpha + 1)\mu^2]. \tag{2}$$

The choice of α in the range $(8\text{–}9)\mu^{-2}$ gives a good description for the experimental data on the $pp \to pn\pi^+$ reaction in the energy range 600–1000 MeV [7].

The πN-scattering amplitude $\Im(z_i, y_i^2; k_i^2)$ and its off-shell behavior was taken according to [2], where the off-shell corrections were introduced into partial waves. We confined ourselves to the P_{33} wave only in the partial wave expansion, assuming the leading role of the 33 resonance in the πN scattering. The partial off-shell 33 amplitude was taken in the form

$$f_{33}(z_i; k_i^2) = \Gamma(k_i^2) f_{33}(z_i; -\mu^2), \tag{3}$$

where $\Gamma(k_i^2)$ is the off-shell correction factor calculated in [2] from dispersion relations, while the on-shell partial f_{33} amplitude was taken in a Breit-Wigner form:

$$f_{33}(z_i; -\mu^2) = \frac{1}{2b_i^s}\gamma[(z^* - z_i) - i\gamma/2]^{-1} \tag{4}$$

with $\gamma = 2\gamma_0(ab_i^s)^3(1 + ab_i^s)^{-2}$, z^*=1232 MeV, $a = 6.3 \times 10^{-3}$ MeV^{-1}, $\gamma_0 = 58$ MeV; b_i^s is the momentum of the proton, scattered on a virtual pion.

The reaction matrix element is a sum of the matrix elements of the corresponding diagrams

$$M = M_A - M_B - M_C + M_D, \tag{5}$$

where the choice of signs is determined by the Pauli principle. All possible interference terms were taken into account. Details of the OPE model we used can be found in [7].

We used a FOWL simulation program [14] in order to obtain all distributions required at once.

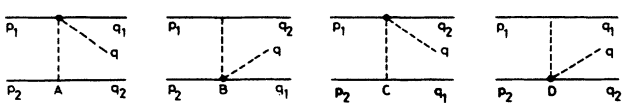

FIG. 1. Feynman diagrams of the OPE model for the $NN \to NN\pi$ reactions.

IV. EXPERIMENTAL RESULTS AND DISCUSSION

The main evidence of the pole diagram contribution would definitely be the observation of the peak in the

distribution on the momentum transfer from the target particle to the secondary proton [e.g., for the diagram A distribution on the $\Delta^2 = -(p_2 - q_2)^2$] at low momentum values. On the other hand, since there is no difference between the final protons in the $pp \to pp\pi^0$ reaction, it is difficult to separate the contribution of a certain diagram experimentally. The whole momentum transfer distribution will be rather complex, because other diagrams have their own singularities. Figure 2 shows, as an example, the contributions of various diagrams to Δ^2 distribution for the incident momentum 1534 MeV/c. The contribution of diagram A really contains the low momentum peak, while the B-diagram contribution has a maximum at high Δ^2. It is quite natural because diagram B has a singularity in $\bar{\Delta}^2 = -(p_1 - q_2)^2$ distribution, so for this diagram the beam proton is a spectator and Δ^2 is not small (p_2 is the nucleon mass in the laboratory system and q_2 is almost equal to p_1). The contributions of diagrams C and D are similar to those of B and A, respectively, but more spread out.

Figure 3 shows the experimental Δ^2 distributions for seven energies together with OPE model predictions (dashed lines) and phase space calculations (broken lines), normalized by the total experimental cross sections. The numerical values of the experimental data for these and the following distributions can be found in the tables of Ref. [28]. The solid lines in Fig. 3 and the following ones present absolute values of the OPE model calculations—they are given only for the lowest and the highest beam energies. One can see that these absolute values do not agree with the experiment (see Table I too). We shall return to this question later when we will discuss the energy dependence of the cross sections. The beam momentum values, given in the figures, correspond to the beam at the chamber entrance and differ by 2 MeV/c on average from the values in Table I.

If we are distracted from the absolute cross-section values, we can see that the OPE model describes qualitatively well experimental data on Δ^2 (Fig. 3) at all energies studied. It is remarkable because one should bear in mind that only the P_{33} wave was taken into account in the πN scattering. Maybe the Δ^2 distribution is sensitive mainly to the pole diagram propagator, and the dependence on the πN amplitude will manifest itself in other distributions.

Figure 4 presents the distributions in momentum transfer from the beam proton to π^0 meson [$r^2 = -(p_1 -$

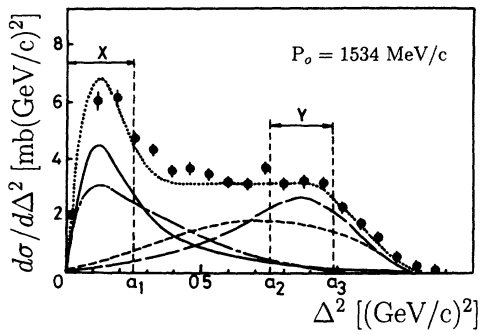

FIG. 2. The contributions of various diagrams to the four-momentum transfer Δ^2 distribution. The solid curve is the contribution of the A diagram, the long dashed curve is that of B diagram, the small dashed and dot-dashed — the contributions of C and D, respectively. The dotted curve shows the sum of all four diagrams normalized to the experimental cross section. X, Y denote intervals in which A and B diagrams dominate, respectively.

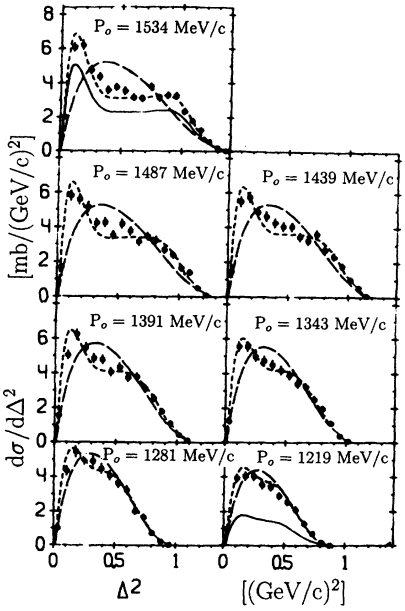

FIG. 3. The four-momentum transfer Δ^2 distributions. The solid curves are the OPE model predictions. The small dashed and dashed curves are the calculations of the OPE model and the phase space normalized to the experimental cross section.

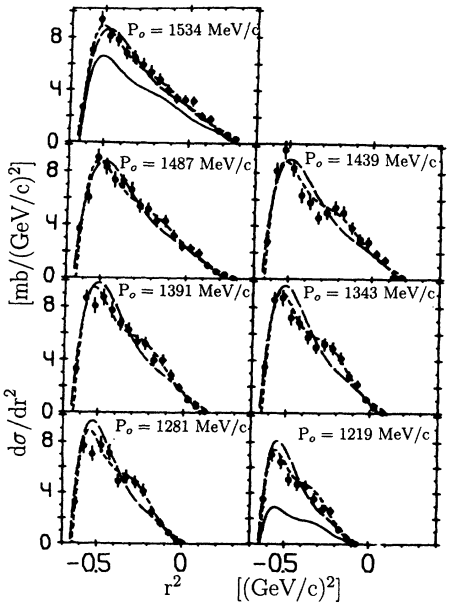

FIG. 4. The four-momentum transfer r^2 distribution. The curves have the same meaning as in Fig. 3.

$q)^2$]. Again one can see the qualitative agreement between the OPE calculations and the experimental data, though these distributions are less sensitive to the model since the phase space curves are also in reasonable agreement with the experiment. One can conclude at least from these data that the contribution of the diagrams with the nucleon exchange is rather small because the experiment does not reveal any peak at low r^2 as compared with the phase space.

One of the criteria of the peripherality of the interaction is the isotropy of the Treiman-Yang angle distribution [15]. It should be isotropic if the process is determined by the exchange of the scalar particle (in our case by a neutral pion). However, because of the indistinguishablity of the final protons (e.g., for diagram A one can take a q_1 proton from the πN-scattering block instead of the q_2 proton) the final Treiman-Yang angle distribution can be distorted. For this reason one should compare the experimental data with the calculations in which all the diagrams of Fig. 1 are taken into account. Figure 5 demonstrates our experimental distributions with expected OPE calculations. One can see the discrepancies between the experiment and model predictions at higher beam energies, which is the evidence that some other mechanism (besides OPE) contributes to the pion production process.

Figures 6 and 7 show the laboratory momentum spectra of final protons and the pion of the $pp \to pp\pi^0$ reaction. In proton spectra one can see two peaks: one is in the region 300–400 MeV/c (independently of the incident energy); the second one moves to the left with the decrease of the beam energy. The low-energy peak corresponds to the target proton as a spectator, while the high-energy one corresponds to the incident proton as a spectator. OPE calculations describe the experiment very well. Pion spectra are close to the phase space distributions and are less representative.

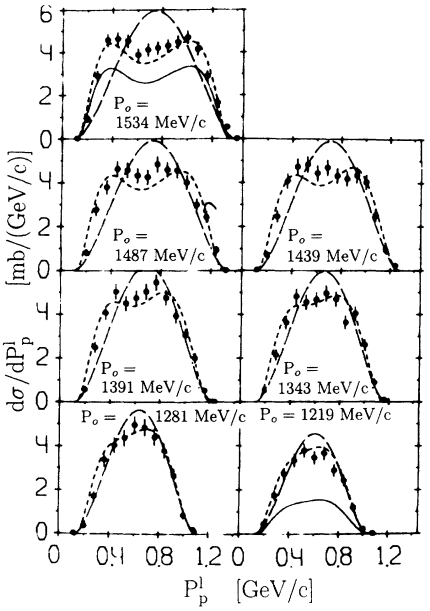

FIG. 6. The laboratory momentum spectra of the final protons. The curves have the same meaning as in Fig. 3.

Figures 8 and 9 show the $M_{p\pi^0}$ and M_{pp} effective mass distributions. It looks like the distributions on $M_{p\pi^0}$ consist of two parts: one is the phase space distribution, while the other has the form of a peak with a width $\sim$100 MeV/c^2. At higher beam energies the peak location corresponds to the Δ_{33} mass. For lower energies, the peak is shifted asymmetrically to the left because of the phase space limitations. The origin of these two contri-

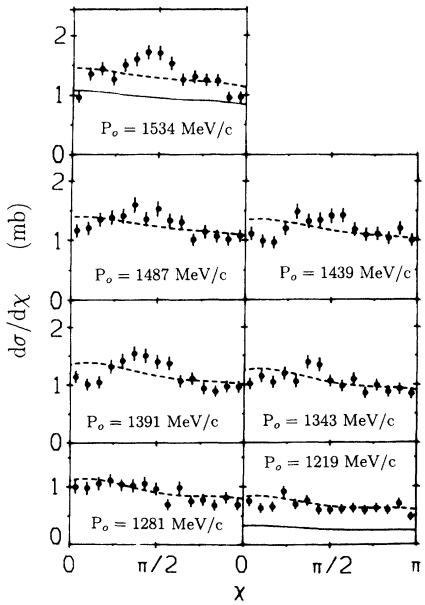

FIG. 5. Treiman-Yang angle distributions. The curves have the same meaning as in Fig. 3.

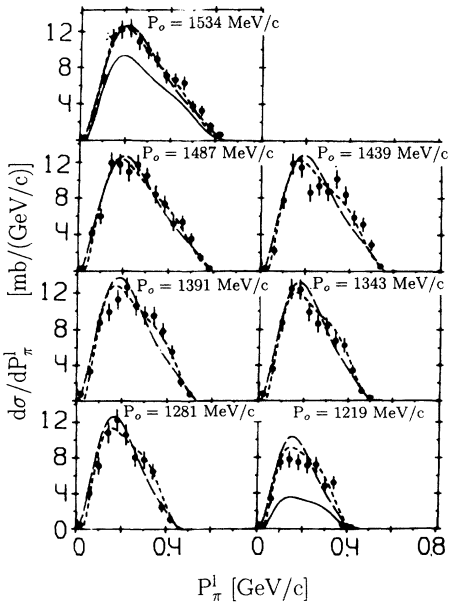

FIG. 7. The laboratory momentum spectra of π^0 mesons. The curves have the same meaning as in Fig. 3.

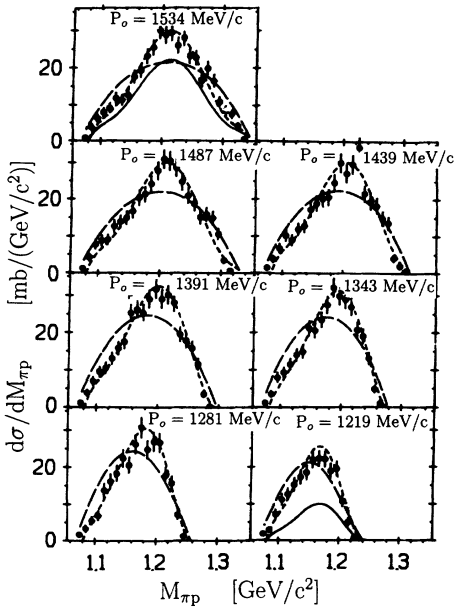

FIG. 8. $p\pi^0$ effective mass spectra. The curves have the same meaning as in Fig. 3.

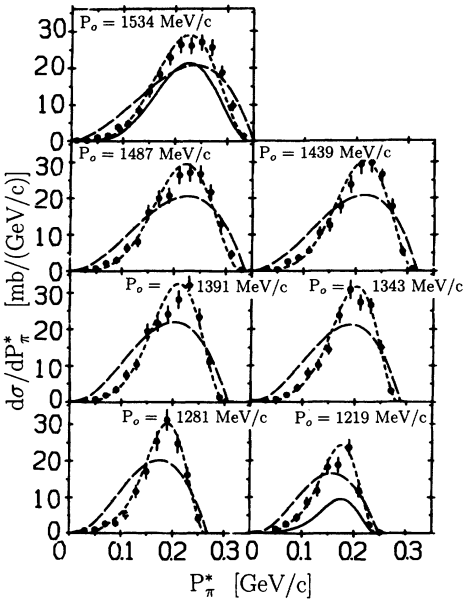

FIG. 10. Momentum spectra (c.m.s.) of π^0 mesons. The meaning of the curves is the same as in Fig. 3.

butions is quite clear in the frame of the OPE model if one keeps in mind that the πN scattering comes from the P_{33} wave only. When the $M_{p\pi^0}$ is calculated for the spectator proton (e.g., q_2 in diagram A, Fig. 1) one has the phase space distribution. When the proton comes from the πN-scattering block the resulting $M_{p\pi^0}$ distribution corresponds to the Δ_{33} isobar peak. Of course, for low energies the isobar production with a mass $\sim$1230 MeV/c^2 is suppressed, but it works effectively down to $\sim$600 MeV due to the isobar width. As can be seen from Figs. 8 and 9, OPE calculations are in qualitative agreement with the experiment at all energies studied. The same situation holds for c.m.s. momentum spectra of pion and protons (Figs. 10 and 11), because these are completely determined by the effective mass distributions.

The angular distributions of pion and protons are given in Figs. 12 and 13. Due to the identity of the initial and final nucleons, the distributions must be symmetrical, so the backward and forward hemispheres were summed up.

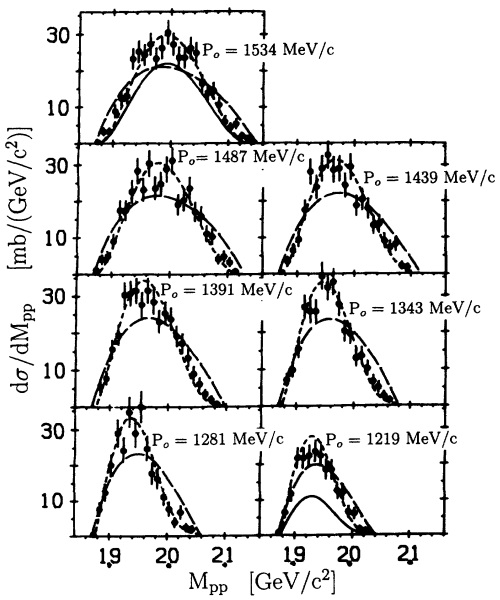

FIG. 9. Effective mass spectra of final protons. The curves have the same meaning as in Fig. 3.

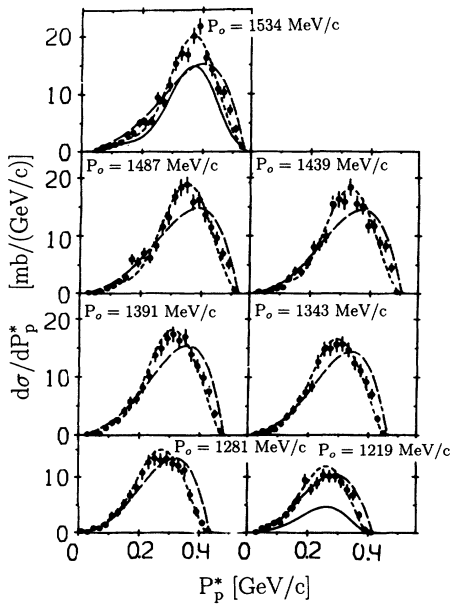

FIG. 11. Momentum spectra (c.m.s.) of final protons. The meaning of the curves is the same as in Fig. 3.

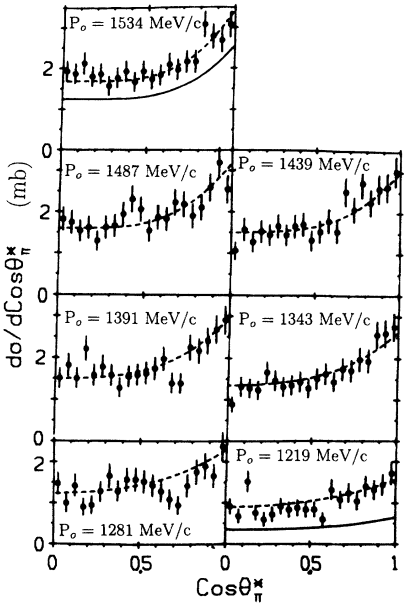

FIG. 12. Proton angular distributions (c.m.s.). The meaning of the curves is the same as in Fig. 3.

OPE calculations are in rather good agreement with the experimental data with the exception of the small proton scattering angles. A possible explanation of this discrepancy is the presence of the only P_{33} wave in the πN-scattering amplitude. It is clear that the small admixture of other waves interfering with the main one should manifest itself mainly in the angular distributions.

Since c.m.s. angular distributions of pions should be symmetrical, we tried to fit them by the formula

$$\frac{d\sigma}{d\Omega^*_{\pi^0}} = \frac{k}{2\pi}(1/3 + b\cos^2\theta^*_{\pi^0}). \qquad (6)$$

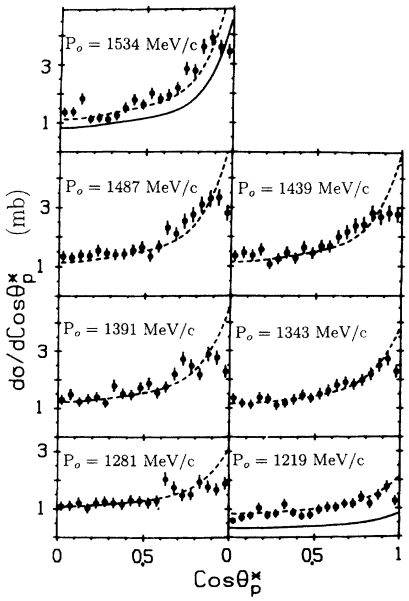

FIG. 13. π^0-meson angular distributions (c.m.s.). The meaning of the curves is the same as in Fig. 3.

The results of such a fit are given in Table II and in Fig. 14 together with the data from other experiments. One should say that the distributions are far from being isotropic: $b \sim 0.2$–0.3 even for low energies. This contradicts the data of [8,9] in the energy region 600–700 MeV. From Table II(a) one can see that the χ^2 value is rather large for low energies. If one includes the additional term $c\cos^4\theta^*_\pi$, the description becomes better [Table II(b)]. This fact might be an indication that pion angular distributions contain powers of $\cos\theta^*_\pi$ higher than 2 with considerable contribution. This problem is important [16], being connected with known attempts to estimate the contribution of the isoscalar channel to the inelastic NN interaction. If this contribution is zero, the angular distributions of charged pions in $np \to pp\pi^-$ $(nn\pi^+)$ reactions should be simular to those of π^0 mesons in the $pp \to pp\pi^0$ reaction. The presence of terms linear in $\cos\theta^*_{\pi^\pm}$ in angular distribution of np reactions might be considered as an indication of the isoscalar contribution. It is clear that to catch a small contribution of the isoscalar channel one needs to know well enough a form of the isovector contribution, for which the $pp \to pp\pi^0$ reaction presents better opportunity. Our statistics, however, is not large enough to obtain reliable values for coefficients at $\cos^2\theta^*_\pi$ and $\cos^4\theta^*_\pi$ simultaneously. One should note that the approximation with $b = 0$, $c \neq 0$ [Table II(c)] gives a better description at low energies than that with $b \neq 0$, $c = 0$.

The opening angle distributions for protons are given in Fig. 15. The OPE predictions for $\cos\theta^*_{pp}$ do not differ much from the phase space distributions.

Figure 16 shows the distributions in $\cos\theta^*_{\pi^0 p}$. As in the case of $\cos\theta^*_{pp}$, the OPE model predictions are in agreement with the experiment at all energies.

Thus we can say that the OPE model with only the P_{33} wave in the πN amplitude describes the experiment well (with the exception, may be, for Treiman-Yang angle distributions). The importance of the P_{33} wave is confirmed also by the $M_{\pi^0 p}$ spectra. An additional evidence for the P_{33}-wave contribution might be obtained by the study

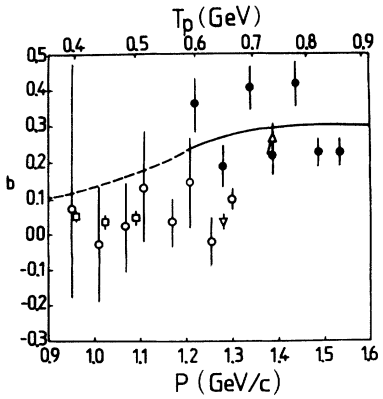

FIG. 14. The values of the parameter b from the fit of the angular distributions (c.m.s.) of the π^0 mesons according to the form $\frac{d\sigma}{d\Omega^*} = (\frac{1}{3} + b\cos^2\theta^*_{\pi^0})$. The curve shows the result of the OPE model calculation. The data are from • - this work, ○ - [8], ▽ - [9], △ - [10], □ - [16].

TABLE II. The results of the π^0-meson c.m.s. angular distribution fitting.

P (MeV)/c	1217	1279	1341	1389	1437	1485	1536
	(a) $d\sigma/d\Omega^*_{\pi^0} = \frac{k}{2\pi}(\frac{1}{3} + b\cos^2\theta^*_{\pi^0})$						
b	0.36±0.07	0.19±0.05	0.41±0.06	0.21± 0.04	0.42±0.06	0.23±0.04	0.23±0.04
χ^2/N_{DF}	1.22	1.33	0.67	1.50	0.72	0.89	0.83
	(b) $d\sigma/d\Omega^*_{\pi^0} = \frac{k}{2\pi}(\frac{1}{15} + \frac{b}{5}\cos^2\theta^*_{\pi^0} + \frac{c}{3}\cos^4\theta^*_{\pi^0})$						
b	−0.04±0.15	−0.11±0.12	0.12±0.13	−0.27±0.09	0.27±0.14	0.10±0.11	−0.09±0.09
c	0.27±0.10	0.22±0.08	0.21±0.08	0.34±0.06	0.11±0.09	0.09±0.08	0.22±0.06
χ^2/N_{DF}	1.12	1.24	0.53	0.88	0.77	0.88	0.53
	(c) $d\sigma/d\Omega^*_{\pi^0} = \frac{k}{2\pi}(\frac{1}{5} + c\cos^4\theta^*_{\pi^0})$						
c	0.25±0.04	0.14±0.03	0.27±0.03	0.17±0.03	0.27±0.03	0.16±0.03	0.16±0.02
χ^2/N_{DF}	1.06	1.22	0.53	1.05	0.83	0.87	0.53

of the π^0 angular distribution in the $\pi^0 p$ rest frame: it should have the form $\sim (1 + 3\cos^2\alpha)$. The experimental distributions are shown in Fig. 17 for all pion-proton combinations. One can see that these distributions do not behave as expected. The deviation is caused by the mixing of final protons, that is confirmed by the agreement between the experiment and the OPE calculations. We tried to select the events for which one diagram, for example A (Fig. 1), gives the dominating contribution. Figure 18 shows the angular distribution for events which have Δ^2 in the X region (see Fig. 2), while other invariant momentum transfers lie in the Y region. One can see that such a selection results in the expected quadratic distribution, though not exactly $1+3\cos^2\alpha$ (one has 1.5–2.5 instead of 3).

Observations of narrow resonance peaks in the M_{pp} spectra in the reaction $np \to pp\pi^-$ were reported in [18], which were considered as candidates to the dibaryon resonances. Our effective mass spectra M_{pp} (Fig. 9) do not reveal any reliable evidences of such peaks. If such peculiarities would exist, they should be independent of the initial energy. Figure 19 shows M_{pp} distributions for the events with the cut in the momentum transfer from the incident proton to π^0 meson, the cut being similar to that used in [18]. Again, one can observe the absence of any energy-stable peculiarities. Thus, we fail to observe any evidence for narrow dibaryon resonances in the pp effective mass spectra in the single pion production.

V. TOTAL CROSS SECTIONS OF THE SINGLE PION PRODUCTION AND THE CHOICE OF THE FORM FACTOR

We tried to understand why the OPE model, which reproduces the form of the differential distributions, fails

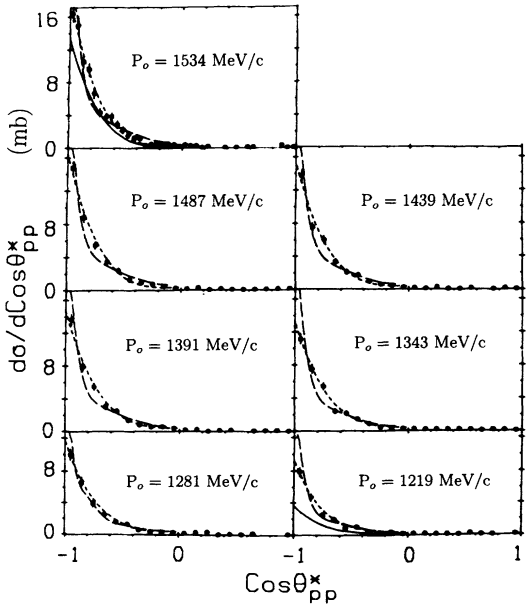

FIG. 15. Center-of-mass opening angle distributions for two protons. The meaning of the curves is the same as in Fig. 3.

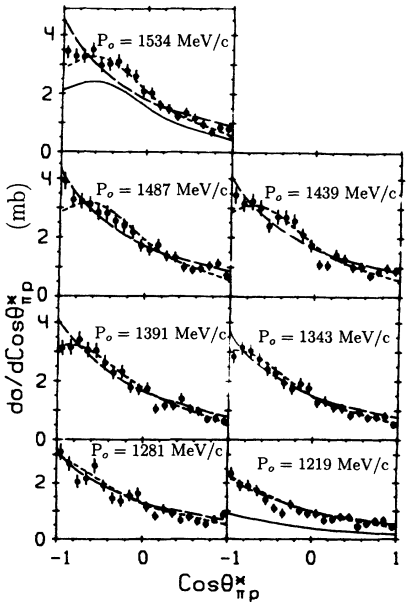

FIG. 16. Center-of-mass opening angle distributions for proton and π^0 meson. The meaning of the curves is as in Fig. 3.

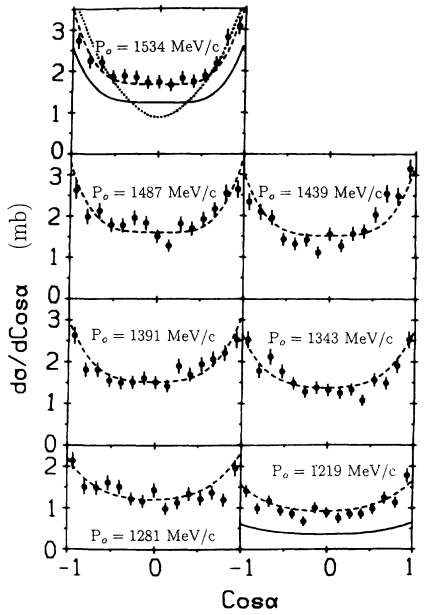

FIG. 17. Distributions of $\cos\alpha$ (the π^0 meson and proton opening angle) in the $\pi^0 p$ rest frame. The meaning of the curves is the same as in Fig. 3. The dotted curve shows the $(1 + 3\cos^2\alpha)$ dependence.

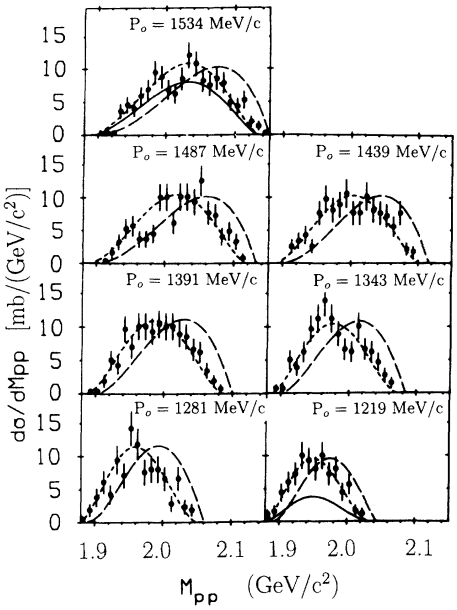

FIG. 19. Effective mass spectra after selecting in r^2. The meaning of the curves is the same as in Fig. 3.

to describe the total cross section values for the $pp \to pp\pi^0$ reaction (Table I). The existing experimental data on the total cross sections are shown in Fig. 20 together with the model predictions. The discrepancy between the theory and experiment is obvious. One can obtain better agreement by proper choice of the form factor, but such a choice destroys the reasonable agreement with the total cross sections of the $pp \to pn\pi^+$ reaction (Fig. 21). One may guess that the reason for such a situation is that the πN amplitude is not good because only the P_{33} wave is taken into account. The dotted curves in Figs. 20 and 21 are the results obtained with the Deck model [6] in which the πN vertex includes all the waves, obtained in the phase-shift analysis [19]. One can see that this does not change the situation significantly. One should keep in mind, however, that with the exception of the P_{33} wave there is no good receipt for the off-shell correction [20],

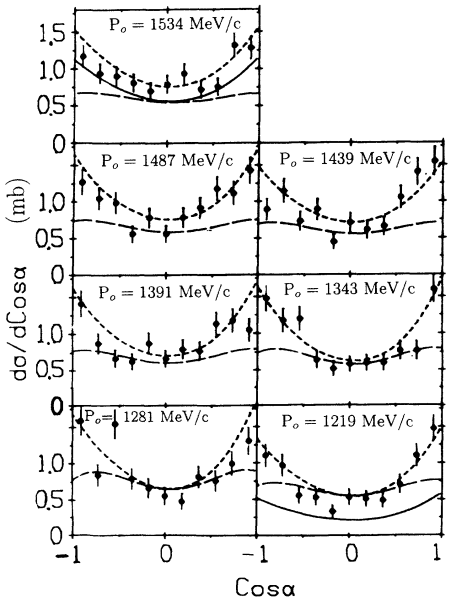

FIG. 18. Distributions of $\cos\alpha$ with the cuts in the momentum transfers and the right choice of final particles. The meaning of the curves is the same as in Figs. 3 and 17.

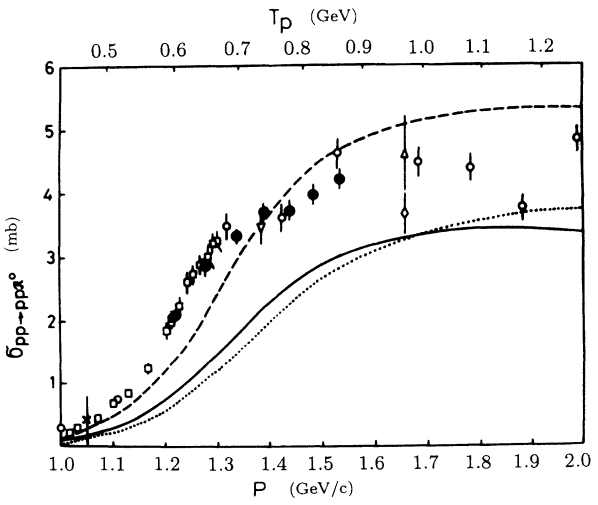

FIG. 20. Cross section of the $pp \to pp\pi^0$ reaction. The solid curve is the OPE model calculation with the P_{33} wave only. The dashed curve—the choice of the form factor to obtain the best fit for the $pp \to pp\pi^0$ reaction. The dotted curve—Deck model calculations [6]. The data are from • - this work, □ - [8], ∇ - [10], ○ - [11], ◇ - [13], △ - [23], × - [24].

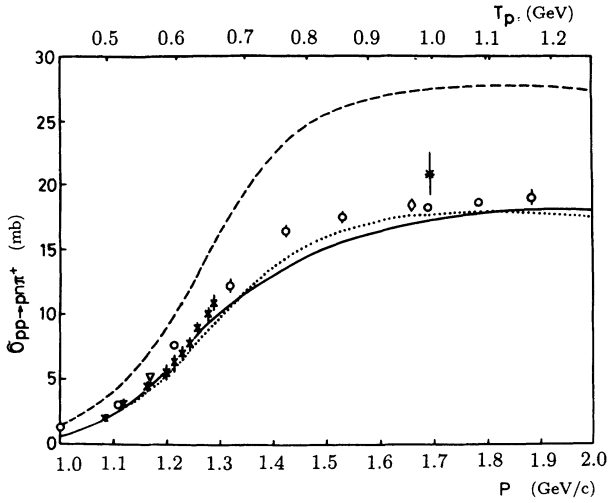

FIG. 21. Cross section of $pp \to pn\pi^+$. The curves are the same as in Fig. 20. The data are from ○ - [11], ◇ - [13], × - [25], ▽ - [26], ∗ - [27].

the correction being very important, as can be seen for the P_{33} wave [21]. So the question remains open.

VI. CONCLUSIONS

A detailed study of differential cross sections of the $pp \to pp\pi^0$ reaction has been performed in the incident energy range 600–900 MeV. The shape of the distributions is described by the OPE model quite well, in spite of the fact that only the P_{33} wave is used in the πN scattering amplitude. The fact that Treiman-Yang angle distributions do not agree well with OPE calculations, may be an indication of some other mechanism contribution to the single pion production. This mechanism does not manifest itself, however, in other differential distributions. On the other hand, the OPE model fails to predict the correct total cross sections, and it cannot be helped by the simple choice of the form factor.

The study of the effective mass spectra gives no evidences for the existence of narrow dibaryon resonances. We can conclude then that if such a six-quark system exists, it represents, most probably, a small admixture in the nuclear matter, because the only candidates to dibaryon resonances were observed in nuclei [22].

ACKNOWLEDGMENTS

We would like to express our deep gratitude to the bubble chamber staff, as well as to the laboratory assistants, which toiled at the film scanning and measuring. We would like to express our thanks to Drs. V. K. Suslenko and I. I. Gaisak for use of the OPE model program and for useful discussions.

[1] S. Mandelstam, Proc. R. Soc. London **A244**, 491 (1958).
[2] E. Ferrary and F. Selleri, Nuovo Cimento **27**, 1450 (1963); **21**, 1028 (1961); F. Selleri, Nuovo Cimento A **40**, 236 (1965).
[3] I.P. Auer *et al.*, Phys. Lett. B **67**, 113 (1977).
[4] M.P. Locher *et al.*, Prog. Part. Nucl. Phys. **16**, 47 (1986).
[5] B.J. Ver West, Phys. Lett. **83B**, 161 (1979).
[6] A. König and P. Kroll, Nucl. Phys. **A356**, 345 (1981); W. Jauch, A. König, and P. Kroll, Phys. Lett. **143B**, 509 (1984).
[7] V.K. Suslenko and I.I. Gaisak, Yad. Fiz. **43**, 392 (1986) [Sov. J. Nucl. Phys. **43**, 252 (1986)].
[8] Y.D. Prokoshkin and A.A. Tyapkin, Zh. Eksp. Teor. Fiz. **32**, 750 (1957) [Sov. Phys. JETP **5**, 618 (1957)]; A.F. Dunaitsev and Y.D. Prokoshkin, *ibid.* **36**, 1656 (1959) [**9**, 1179 (1959)].
[9] V.M. Guzhavin *et al.*, Zh. Eksp. Teor. Fiz. **46**, 1245 (1964) [Sov. Phys. **19**, 847 (1964)].
[10] R.J. Cence *et al.*, Phys. Rev. **131**, 2713 (1963).
[11] F. Shimizu *et al.*, Nucl. Phys. **A386**, 571 (1982).
[12] V.P. Andreev *et al.*, Z. Phys. A **329**, 371 (1988).
[13] D.V. Bugg *et al.*, Phys. Rev. **133**, 1017 (1964).
[14] FOWL, CERN program library, F. James, Th68-15, 1968.
[15] S.B. Treiman and C.N. Yang, Phys. Rev. Lett. **8**, 140 (1962).
[16] S. Stanislav, Ph.D. Thesis, University of British Columbia, Vancouver, 1987.
[17] M. Kleinschmidt *et al.*, Z. Phys. **A 298**, 253 (1980); H. Fisher *et al.*, SIN Newsletter **20**, 15 (1987).
[18] Y.A. Troyan *et al.*, JINR Short Reports No. 13, Dubna, 1985 (unpublished).
[19] G. Höhler, *Handbook of Pion-Nucleon Scattering* (Fachinformationszentrum, Karlsrue, 1979).
[20] M.S. Reiner, Ann. Phys. **154**, 24 (1984).
[21] V.K. Suslenko *et al.*, JINR Report No. P2-88-113, Dubna, 1988 (unpublished).
[22] Ya. Balgansuren *et al.*, JINR Report No. PI-88-503, Dubna, 1988 (unpublished).
[23] A.P. Batson *et al.*, Proc. R. Soc. London **A251**, 233 (1959).
[24] M.S. Kozodoev *et al.*, Proc. Acad. Science USSR **19**, 589 (1955).
[25] B.S. Neganov and O.V. Savchenko, Zh. Eksp. Teor. Fiz. **32**, 1265 (1957) [Sov. Phys. JETP **5**, 1033 (1957)].
[26] T.H. Fields *et al.*, Phys. Rev. **109**, 1713 (1958).
[27] V.G. Vovchenko *et al.*, Yad. Fiz. **24**, 1161 (1976) [Sov. J. Nucl. Phys. **24**, 608 (1976)].
[28] V.P. Andreev *et al.*, Report No. LNPI-1453, St. Petersburg, 1989 (unpublished).